Target-induced Trivalent G-quadruplex/hemin DNAzyme for Colorimetric Detection of Hg^{2+} Based on an Exonuclease III Assisted Catalytic Hairpin Assembly

Zhenghua LIU[1,2], Zhonghai LI[1]*

1. College of Food Science and Engineering, Central South University of Forestry and Technology, Changsha, 410004, China; 2. Technology Center of Changsha Customs District of People's Republic of China, Changsha, 410004, China

Abstract Mercury ion (Hg^{2+}), a highly noxious of heavy metalion, has detrimental effects on the ecological environment and human health. Herein, we have developed an exonuclease III (Exo III) assisted catalytic hairpin assembly formation of a trivalent G-quadruplex/hemin DNAzyme for colorimetric detection of Hg^{2+}. A hairpin DNA (Hr) was designed with thymine-Hg^{2+}-thymine pairs that catalyzed by Exo III is prompted to happen upon binding Hg^{2+}. A released DNA fragment triggers the catalytic assembly of other three hairpins (H1, H2, and H3) to form many trivalent G-quadruplex/hemin DNA enzymes for signal output. The developed sensor shows a dynamic range from 2 pM to 2 μM, with an impressively low detection limit of 0.32 pM for Hg^{2+} detection. Such a sensor also has good selectivity toward Hg^{2+} detection in the presence of other common metal ions. This strategy shows the great potential for visual detection with portable type.

Key words G-quadruplex/hemin DNAzyme; Multivalence; Catalytic hairpin assembly; Exonuclease III; Signal amplification; Colorimetric detection

DOI:10.19759/j.cnki.2164 - 4993.2024.01.013

Mercury ion (Hg^{2+}) has attracted growing attention due to its bioaccumulation and high toxicity[1]. The bioaccumulation of Hg^{2+} has posed serious threats to human health even at very low concentrations, resulting in kidney damage, nervous system disruption, and other malignant diseases[2-4]. Diet is considered a major source of exposure to Hg^{2+}[5]. Consequently, numerous countries and regions have established the maximum allowable concentration (MAC) in food. For instance, the United States Environmental Protection Agency sets the MAC of Hg^{2+} in drinking water at 10 nM[6]. It is imperative to develop a sensitive and accurate analytical technique for Hg^{2+} detection. To meet this need, various instrumental methods such as inductively coupled plasma mass spectrometry (ICP-MS)[7], surface-enhanced Raman (SER)[9], atomic absorption spectroscopy(AAS)[8], and atomic fluorescence spectroscopy (AFS)[10], have been employed for Hg^{2+} detection. However, their usage is limited in standard laboratories because of bulky apparatus, long washing processes, high costs, and the requirement for trained personnel. Therefore, the development of new sensors with high sensitivity, superior selectivity, user-friendliness, and equipment-free capabilities for Hg^{2+} detection remains a valuable challenge.

Artificial deoxyribonucleic acid (DNA) is able to bind targets with high affinity and specificity, making it an ideal candidate for designing highly selective sensors[11-12]. Based on the discovery that trace amounts of Hg^{2+} have a high affinity to bind the thymine-thymine (T-T) mismatched base pairs and can form stable T-Hg^{2+}-T base pairs that fold single-stranded DNA (ssDNA) sequences into duplexes[13-14]. This provides a justification for using T-containing DNA sequences to detect Hg^{2+}. Colorimetric assay is widely applied for Hg^{2+} detection due to its fast response, broad linear range, and simplicity[15]. Various colorimetric assays were developed to detect Hg^{2+}[16-17]. However, the high limit of detection (LOD) in colorimetric assays generally limits their efficacy for trace target detection[18]. To address this challenge, strategies to reducethe LOD of colorimetric assay are developed. For example, Li *et al.* [19] reported a multivalent sensing platform for the detection of Hg^{2+} based on a dual Mg^{2+}-dependent-DNAzyme. The results indicated a significant increase in sensitivity (4.50-fold) and selectivity (1.44-fold) compared to its monomeric counterpart. Heand co-workers demonstrated an electrochemical biosensor for ultrasensitive Hg^{2+} detection using a triple signal amplification strategy, displaying high sensitivity and excellent specificity[20].

Exonuclease III (Exo III) selectively cleaves the double-stranded DNA (dsDNA) with a blunt or recessed 3'-terminus, with no activity on ssDNA or dsDNA with a protruded 3'-terminus[21-22]. It is widely used as an enzymatic tool to facilitate signal transduction and amplification for developing sensitive analytical assays. In this study, we developed a trivalent G-quadruplex/hemin DNAzyme (TDNAzyme) as a high activity peroxidase-like mimic for colorimetric detection of Hg^{2+}. To construct this sensor, the 3'-terminus, and 5'-terminus of a hairpin probe (Hr) were carefully designed to contain thymine-rich sequences that can hybridize with each other in the presence of Hg^{2+}. Then, Exo IIIcatalyzed

Received: December 5, 2023 Accepted: February 6, 2024

Supported by The Science and Technology Project of General Administration of Quality Supervision, Inspection and Quarantine (2015IK126); The Science and Technology Project of Changsha City of Hunan Province of China (KQ1602124).

Zhenghua LIU (1981 -), male, P. R. China, senior engineer, PhD, devoted to research about quality and safety of imported and exported food.

* Corresponding author.

the stepwise removal of mononucleotides from the 3'-terminus, and released a trigger DNA fragment (F). The released F was subsequently recycled through a catalytic hairpin assembly (CHA) process to form many TDNAzymes. The assumption is that the TDNAzymes possess high activity for H_2O_2 catalysis due to multivalent effects[23]. The high catalytic activity suggests the potential for enhanced signal output[24]. Therefore, we believed that a high colorimetric signal can be obtained due to the high catalytic activity of the TDNAzymes and strong signal amplification capability of Exo III assisted CHA[25].

Materials and methods

Reagents and Materials

Mercury (II) nitrate standard solutions were purchased from Beijing North Weiye Institute of Measuring and Testing Technology (China). Exo III and 10 × NE Buffer were purchased from New England Biolabs, Inc. (USA). Hemin was purchased from Sangon Biotech (Shanghai) Co., Ltd. (China), it was dissolved in dimethyl sulfoxide (DMSO) to make a stock solution and diluted with 25 mM HEPES (200 mM NaCl, 20 mM KCl, 0.05% Triton X-100,1% DMSO, pH = 8.4) before use. Ammonium persulfate (APS) and N, N, N', N'-tetramethylethylenediamine (TEMED) were purchased from USB Corporation. GelRed was purchased from US Everbright Inc. (UE). 4, 4'-Diamino-3, 3', 5, 5'-tetramethylbiphenyl sulfate (TMB) was purchased from Aladdin Bio-Chem Technology Co., LTD (China). All DNA oligonucleotides were synthesized by Sangon Biotech (Shanghai) Co., Ltd. (China), and dissolved in Tris-HCl buffer (100 mM NaCl, 20 mM KCl, 20 mM $MgCl_2$, pH7.4). The detailed sequences of the oligonucleotides are listed in Table 1. All other regents were analytical grades and used without further purification. All solutions were prepared and diluted using ultrapure water (≥18.2 MΩ · cm) unless specific description.

Table 1 Sequences of DNA probes

Probes	Sequences (5'-3')
Hc	**TTGATT**TAATCA GCGGGT GACTTA GCGGGT CACATT TAAGTC ACCCGC TGATTA **TTTCTT**
H1	TGGGTAGG GCGGGT GACTTA GCGGGT TGTTCA GCGGGT ACCCGC TAAGTC ACCCGC TGATTA ATGGGT
H2	TGGGTAGG GCGGGT TGTTCA GCGGGT TAATCA GCGGGT ACCCGC TGAACA ACCCGC TAAGTC ATGGGT
H3	TGGGTAGG GCGGGTTTGCTT GCGGGT GACTTG GCGGGT ACCCGC AAGCAA ACCCGC TGTTCA ATGGGT
H1"	$(N)_8$ GCGGGT GACTTA GCGGGT TGTTCA GCGGGT ACCCGC TAAGTC ACCCGC TGATTA ATGGGT
H2"	TGGGTAGGGCGGGT TGTTCA GCGGGT TAATCA GCGGGT ACCCGC TGAACA ACCCGC TAAGTC $(N)_6$
H3"	TGGGTAGG GCGGGTTTGCTT GCGGGT GACTTG GCGGGT ACCCGC AAGCAA ACCCGC TGTTCAATGGGT
H1'	$(N)_8$GCGGGT GACTTA GCGGGT TGTTCA GCGGGT ACCCGC TAAGTC ACCCGC TGATTA ATGGGT
H2'	$(N)_8$GCGGGT TGTTCA GCGGGT TAATCA GCGGGT ACCCGC TGAACA ACCCGC TAAGTC $(N)_6$
H3'	TGGGTAGG GCGGGTTTGCTT GCGGGT GACTTG GCGGGT ACCCGC AAGCAA ACCCGC TGTTCA$(N)_6$

The underlined bases indicate the stem complementary sequence of the hairpin. Bold bases indicate the mismatched bases.

Polyacrylamide gel electrophoresis analysis

2.5 ml acrylamide (40%) and bis-acrylamide solution (19 : 1), 2 ml 5 × TBE buffer, 100 μl APS (10%), 10 μl TEMED, and 6.89 ml ultrapure water were mixed to prepare the gel (10%). The samples were mixed with 6 × loading buffer (2 μl) and subjected to the nondenaturing polyacrylamide gel electrophoresis (PAGE). The PAGE was carried out in 1 × TBE at 120 V for 40 min. After staining in diluted Gel-Red Nucleic Acid Gel Stai, the gel was scanned using a Bio-Rad GelDoc XR imaging system (Bio-Rad, USA).

Detection of Hg^{2+}

Different concentrations of Hg^{2+} were incubated with Hr (250 nM), H1 (250 nM), H2 (250 nM), and H3 (250 nM). Subsequently, Exo III (25 U) was introduced to the solution and incubated at 37 ℃ for 60 min, followed by incubation with hemin (500 nM) for 30 min. TMB and H_2O_2 were then added to the solution and the reaction was terminated by the addition of H_2SO_4 (2 M). The absorbance was measured by a spectrophotometer at 450 nm (UV-2450, Shimadzu, Japan).

Detection of Hg^{2+} in real samples

To assess the effectiveness of TDNAzymes for detecting Hg^{2+} in real samples, tap water from the laboratory, and commercially purchased milk were utilized in this study. Certain amounts of Hg^{2+} were spiked into these real samples[19]. The sample preparation steps were as follows: (a) For the spiked milk sample: 3 ml of the spiked milk sample, 1 ml of HNO_3 (65%, *v/v*), and 2 ml of H_2O_2 (30%, *v/v*) were added in a 50 ml flask. The mixture was heated at 120 ℃ until it became a clear solution. The solution was allowed to cool to room temperature, and the pH value was adjusted to 7.4 using the sodium hydroxide solution. The solution was then filtered through a 0.22 μm filter membrane. (b) The spiked tap water was filtered through a 0.22 μm filter membrane. After that, all spiked samples were added to reaction solutions (the final concentrations of Hg^{2+} were 0.20, 5.00, and 100.00 nM). At the same time, the final solutions were measured by an Atomic Fluorescence Spectrophotometer (Beijing Purkinje General Instrument Co., Ltd., China).

Results and Discussion

Design strategy for Hg^{2+} detection

The design strategy that the highly active TDNAzyme for colorimetric detection of Hg^{2+} based on the ExoIII assisted CHA was illustrated in Fig. 1. Where, four hairpin probes (Hr, H1, H2, and H3), and Exo III were utilized to construct the sensing system. Hr was designed with protruded 3'-terminus and 5'-terminus resistant Exo III cleavage. Simultaneously, these termini contained

thymine-rich sequences capable of hybridizing in the presence of Hg^{2+}. To inhibit the assembly formation of the highly active TDNAzyme, the enzymatic sequence was divided into two parts and separately inserted at the 3'-terminus and 5'-terminusof other three hairpins (H1, H2, and H3). Consequently, in the absence of Hg^{2+}, all hairpin probes maintained stable closed conformations, and the self-assembly process did not occur due to inhibited enzymatic hydrolysis of Hr. In the presence of Hg^{2+}, the protruding sticky termini of Hr formed a rigid DNA hairpin with a blunt 3'-terminus. Exo III catalyzed the stepwise removal of mononucleotides from the 3'-terminus of Hr. After complete consumption of the duplex stem, Hg^{2+} was released to initiate the next round of cleavage, and a DNA fragment (T) was generated to service as a trigger for catalytic hairpin assembly (CHA). This process produced numerous TDNAzymes. Eventually, the two parts of DNAzyme sequences were brought into close proximity, binding with hemin to form a peroxidase-mimicking G-quadruplex/hemin DNAzyme. The active G-quadruplex/hemin DNAzyme effectively catalyzed the H_2O_2-mediated oxidation of TMB, generating a colored output signal. Through the two-step circling amplification, a strategy for the colorimetric detection of Hg^{2+} by Exo III assisted CHA was achieved.

Feasibility of the sensing system

To verify the feasibility of the TDNAzyme-based assay for Hg^{2+} detection, Fig. 2A illustrates the absorption spectrum of detection solutions under different conditions. In the absence of Hg^{2+}, the detection solution showed a negligible response (black curve), indicating that Hr could not be digested by Exo III due to the T-T mismatched base pairs. Consequently, F was not released to induce a CHA reaction for forming the TDNAzyme. Notably, when Hg^{2+} was present in the detection solutions, the absorption signal dramatically increased (red curve). This result indicated that Hg^{2+} induced a hybridization reaction between the 3'-terminus and 5'-terminus of Hr, promoting Exo III digestion and generating numerous F. Then, F was recycled through a CHA process to form many TDNAzymes for signal output. These results clearly demonstrated the feasibility of this strategy in providing an amplified signal for Hg^{2+} detection.

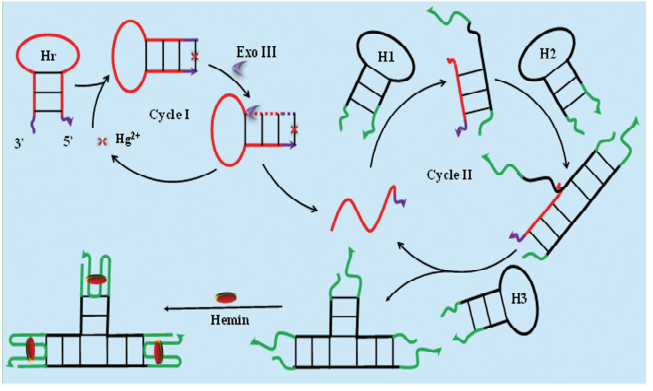

Fig. 1 Principle of the TDNAzyme-based assay for colorimetric Hg^{2+} detection

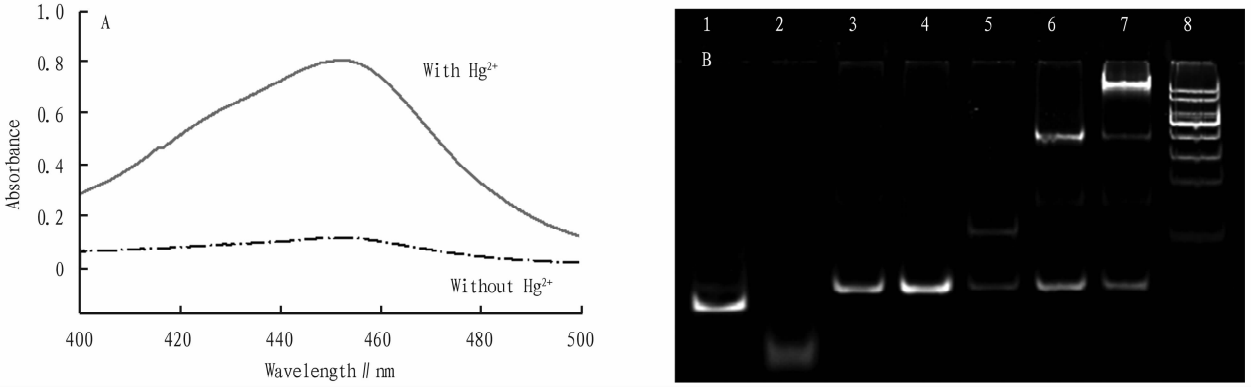

(A) The absorbance spectra of detection solutions with(red curve) or without Hg^{2+} (black curve). The mixtures were allowed to react at 37 ℃ for 60 min. (B) PAGE characterization of the forming process of TDNAzyme. Lane 1: Hr, and Exo III; Lane 2: Mixture of Hr, Exo III, and Hg^{2+}; Lane 3: H1; Lane 4: H1, H2, and H3; Lane 5: Hr, H1, Hg^{2+}, and Exo III; Lane 6: Hr, H1, H2, Hg^{2+}, and Exo III; Lane 7: Hr, H1, H2, H3, Hg^{2+},and Exo III; Lane 8: Mark. The concentrations of Hr, H1, H2, H3, Exo III, and Hg^{2+} were 250 nM, 250 nM, 250 nM, 250 nM, 25 U, and 200 nM, respectively.

Fig. 2 The feasibility of the TDNAzyme-based assay to detect Hg^{2+}

Polyacrylamide gel electrophoresis analysis (PGEA) was employed to validate the TDNAzyme-based assay for Hg^{2+} detection, as depicted in Fig. 2B. In Lane 1, a bright band corresponding to Hr was observed. When Hg^{2+} was introduced to a mixture of Hr and Exo IIIin Lane 2, a new band appeared with a faster migration rate than that inLane 1. Simultaneously, the band corresponding to Hr was nearly present. These results indicated that T-Hg^{2+}-T base pairs created a cleavage site for Exo III, resulting in a low molecular weight digestion product. The band in Lane 3 corresponded to H1, while Lane 4 represents to the mixture of H1, H2, and H3. These bands exhibited almost identical migration rates. Upon mixingHg^{2+}, Hr, and Exo III with H1, a band corresponding to the product H1-Fwas observed (Lane 5). After H2 was introduced, a new band corresponding to H1-F-H2 was observed (Lane 6). Subsequently, upon addition of H3, a bright band with much lower mobility that corresponded to H1-H2-H3 complex was

observed (Lane 7), suggesting the successful formation of the TDNAzyme. These results strongly suggested that nucleic acid hybridizations in CHA can be successfully proceeded.

Catalytic activity of TDNAzymes

Multivalency greatly enhances the catalytic activity of G-quadruplex/hemin DNAzymes[23]. We hypothesized that the TDNAzymes have enhanced catalytic activity due to the multivalent effect. To test this hypothesis, control experiments with different valence numbers of DNAzymes under the same conditions were performed. As shown in Fig. 3, a monovalent G-quadruplex/hemin DNAzyme exhibited a weak absorption signal, indicating low catalytic activity for the TMB substrate. We inferred the large molecular weight DNA complex prevents the binding of the enzyme stand to the substrate[26]. After introducing the bivalent G-quadruplex/hemin DNAzyme, the absorption signal significantly increased. When the TDNAzyme was added, the absorption signal was greatly improved. Therefore, the multivalent effect can be used to enhance the catalytic activity of the substrate.

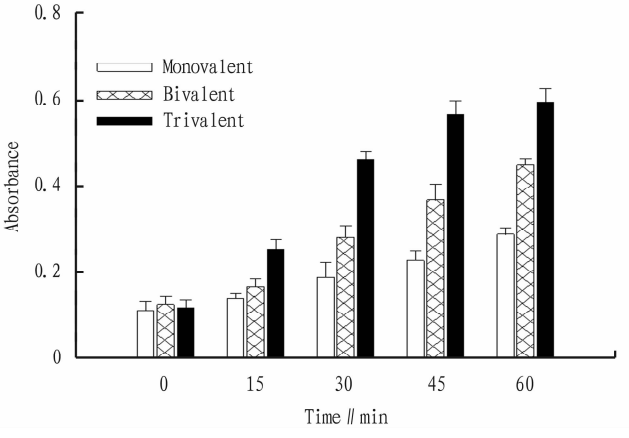

The concentration ratio of monovalent-, bivalent-, and trivalent-G-quadruplex/hemin DNAzymes was 6∶3∶2. Error bars indicate the standard deviations of three experiments.

Fig. 3 Effects of valence numbers of G-quadruplex/hemin DNAzyme on catalytic activity for TMB substrate

Optimization of experimental conditions

The results of this experiment are affected by various conditions such as the reaction temperature, concentrations of H1, H2, and H3, reaction time of Exo III, and the concentration of Exo III. In order to achieve the best sensing performance for the TDNAzyme-based assay, the ratio of A/A0 was employed to establish the optimal experimental conditions, where A and A0 represent the absorption intensities of the assay in the presence and absence of Hg^{2+}, respectively.

The reaction temperature significantly influenced the activity of Exo III. Thus, the effect of different reaction temperatures (15 −45 ℃) was investigated. As shown in Fig. 4, in the presence of Hg^{2+}, the ratio of A/A0 increased with reaction temperature in the range from 15 to 37 ℃ and then decreased in the range from 37 to 45 ℃. The result indicated that the low temperature could affect the activity of Exo III, while high temperature influenced the stability of Hr. Therefore, 37 ℃ was considered for the best A/A0 in our study.

The reaction time of Exo III is a key factor for the sensing system. Thus, the reaction time of Exo III was optimized. As shown in Fig. 5, it was evident that the A/A0 increased with the reaction time, and reached a maximum at 60 min. Thus, 60 min was chosen as the optimal reaction time of Exo III.

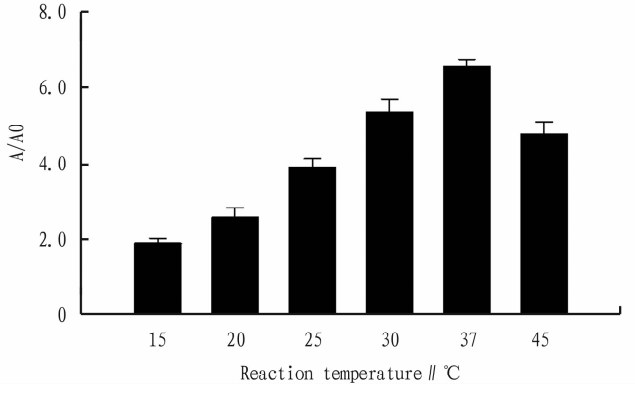

The absorbance was obtained in the presence of 20 nM Hg^{2+}. The error bars represent the standard deviation of three parallel measurements.

Fig. 4 Effect of reaction temperature on A/A0

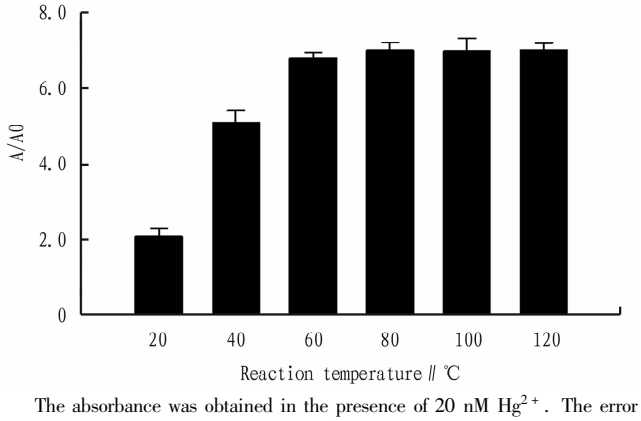

The absorbance was obtained in the presence of 20 nM Hg^{2+}. The error bars represent the standard deviation of three parallel measurements.

Fig. 5 Effect of the reaction time on A/A0

To achieve an excellent signal amplification effect, the concentration of Exo III was optimized. When the concentration of Exo III was less than 25U, A/A0 increased rapidly with the increasing concentration of Exo III. However, due to the limited concentration of Hr, the reaction was saturated in 25U of Exo III (Fig. 6). Therefore, the optimal concentration of Exo III was determined to be 25U.

It is noteworthy that the concentrations of H1, H2, and H3 have a crucial effect on the efficiency of amplification. Thus, the concentrations of H1, H2, and H3 were optimized. As shown in Fig. 7, it was evident that the optimized concentrations of H1, H2, and H3 are 250 nM. To achieve good sensitivity, we chose 250 nM of H1, H2, and H3 in the following experiments.

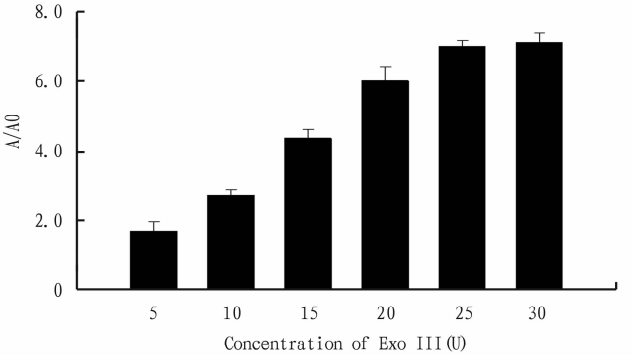

The absorbance was obtained in the presence of 20 nM Hg^{2+}. The error bars represent the standard deviation of three parallel measurements.

Fig. 6 Effect of the concentration of exonuclease III (Exo III) on A/A0

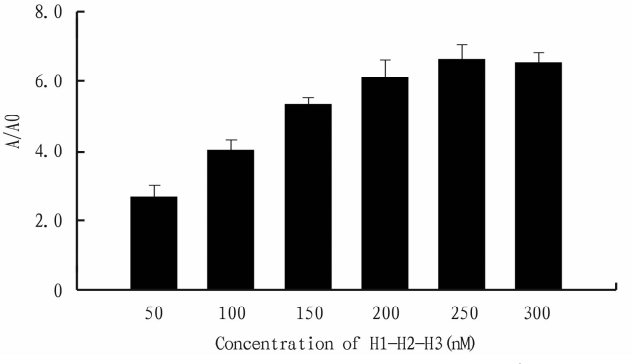

The absorbance was obtained in the presence of 20 nM Hg^{2+}. The error bars represent the standard deviation of three parallel measurements.

Fig. 7 Effect of the concentration of H1-H2-H3 on A/A0

Performance of the sensing system

After optimizing the reaction conditions in the experiments, we further investigated the performance of the sensing system at different concentrations of Hg^{2+}. Fig. 8A displays the increased absorption signal with an elevated amount of Hg^{2+} ranging from 0 to 2 μM. A high linear correlation was obtained between the absorption intensity and the logarithm of Hg^{2+} concentration over 6 orders of magnitude in the range of 2 pM to 2 μM. The calibration curve with the equation of $y = 0.049\ 7\lg c + 0.622\ 7$ ($R^2 = 0.991\ 1$) was obtained for Hg^{2+} detection (Fig. 8B), where y is the absorption intensity, and c is the Hg^{2+} concentration. The LOD corresponding to three times the standard deviation of the blank was found to be 0.32 pM, which is close to or even better than some of the previously reported methods (Table 2).

Table 2 Comparison of the sensing system with other reported assays

Method	Linear range	LOD	Ref.
Electrochemical	10 pM – 100 μM	2.9 pM	[1]
Fluorescent	0.02 – 200 μM	2.6 nM	[2]
Fluorescent	10 fM – 100 nM	10.0 fM	[3]
Fluorescent	10 – 100 nM	0.68 nM	[4]
Colorimetric	1.0 – 50 nM	0.23 nM	[5]
Colorimetric	2 pM to 2 μM	0.32 pM	This work

It is note worthy that the concentrations of H1, H2, and H3 have a crucial effect on the efficiency of amplification. Thus, the concentrations of H1, H2, and H3 were optimized. As shown in Fig. 7, it was evident that the optimized concentrations of H1, H2, and H3 are 250 nM. To achieve good sensitivity, we chose 250 nM of H1, H2, and H3 in the following experiments.

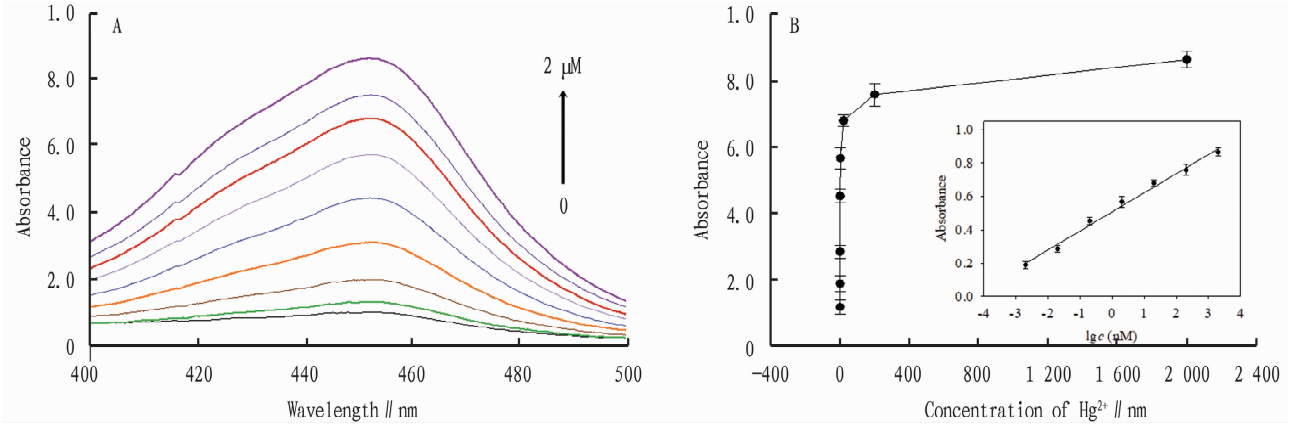

(A) The UV-vis absorption peaks corresponding to the detection solutions at different concentrations of Hg^{2+} (0, 0.2, 2, 20, 200 pM, 2, 20, 200, and 2 μM). (B) Plot of absorption intensity vs concentrations of Hg^{2+}.

Inset is a linear relationship between the absorption signal and the logarithm of Hg^{2+} concentrations in the range from 2 pM to 2 μM. Error bars indicate the standard deviations of three experiments.

Fig. 8 UV-vis absorption peaks of detection solutions

Application to real samples

To further estimate the practical applicability of TDNAzymes for the detection of Hg^{2+}, several real samples including tap water, and milk were analyzed. Hg^{2+} was not detected in these real samples. Subsequently, different concentrations of Hg^{2+} standard solutions were spiked into the real samples to evaluate the recoveries of the proposed method. The results are shown in Table 3, the recovery rates of Hg^{2+} range from 95.00% to 108.33%, with the relative standard deviation (*RSD*) in the range of 3.66% – 10.53%. These results are similar to AFS which is the standard method for

the detection of Hg^{2+}. These results suggested that the proposed method is suitable for Hg^{2+} detection in real samples.

Conclusions

In summary, we developed a highly active TDNAzyme for colorimetric detection of Hg^{2+} based on Exo III assisted CHA, which has several significant advantages. Firstly, compared with the monovalent G-quadruplex/hemin DNAzyme that suffers from unsatisfied signal output, TDNAzyme demonstrates enhanced signal amplification efficiency. This enhancement allows for the rapid analysis of Hg^{2+} at the picomole level and performs effectively in real samples. Secondly, the experimental operation is greatly simplified through a one-pot reaction strategy, indicating the TDNAzyme-based assay has the potential to be used by non-professionals. Third, the colorimetric method is operated with equipment-free, which provides a practical solution for screening the food contaminated with Hg^{2+}, especially in remote areas.

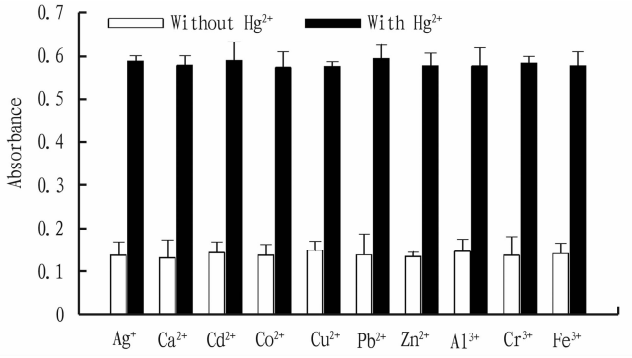

Error bars indicate the standard deviations of three experiments.

Fig. 9 Selectivity assay of the TDNAzyme-based assay upon the addition of Hg^{2+} (2 nM) and various interfering ions (2 nM)

Table 3 Determination of Hg^{2+} in real samples using the proposed method and AFS

Sample	Add//nM	This work			AFS		
		Found//nM	Recovery//%	RSD//%	Found//nM	Recovery//%	RSD//%
Tap water	0.20	0.19	95.00	10.53	0.20	101.67	5.68
	5.00	4.91	98.27	5.42	4.99	99.87	2.54
	100.00	101.64	101.64	4.48	102.99	102.99	4.98
Milk	0.20	0.22	108.33	11.62	0.20	100.00	8.66
	5.00	4.93	98.53	3.66	4.98	99.53	2.62
	100.00	106.53	106.53	8.40	103.46	103.46	5.74

References

[1] RASHID S, SHAH IA, TULCAN RXS, *et al.* Contamination, exposure, and health risk assessment of Hg in Pakistan: A review[J]. Environ. Pollut., 2022(301): 118995.

[2] HUANG Y, LI Y, LI Y, *et al.* An "AIE + ESIPT" mechanism-based benzothiazole-derived fluorescent probe for the detection of Hg^{2+} and its applications[J]. New J. Chem., 2023(47): 6916 – 6923.

[3] WU H, XIE R, HAO Y, *et al.* Portable smartphone-integrated AuAg nanoclusters electrospun membranes for multivariate fluorescent sensing of Hg^{2+}, Cu^{2+} and l-histidine in water and food samples[J]. Food Chem., 2023(418): 135961.

[4] HAO GUO NW, PENG L, CHEN Y, *et al.* A novel ratiometric fluorescence sensor based on lanthanide-functionalized MOF for Hg^{2+} detection [J]. Talanta, 2022(250): 123710.

[5] ÖZYURT C, ÜSTÜKARCI H, EVRAN S, *et al.* MerR-fluorescent protein chimera biosensor for fast and sensitive detection of Hg^{2+} in drinking water [J]. Biotechnol. Appl. Biochem., 2019(66): 731 – 737.

[6] GAUTHAMA B, NARAYANA B, SAROJINI B, *et al.* Colorimetric "off-on" fluorescent probe for selective detection of toxic Hg^{2+} based on rhodamine and its application for in-vivo bioimaging[J]. Microchem. J., 2021 (166): 106233.

[7] JINADASA KK, HERBELLO-HERMELO P, PEÑA-VÁZQUEZ E, *et al.* Mercury speciation in edible seaweed by liquid chromatography-Inductively coupled plasma mass spectrometry after ionic imprinted polymer-solid phase extraction[J]. Talanta, 2021(224): 121841.

[8] GHAEDI M, REZA FATHI M, SHOKROLLAHI A, *et al.* Highly selective and sensitive preconcentration of mercury ion and determination by cold vapor atomic absorption spectroscopy[J]. Anal. Lett., 2006 (39): 1171 – 1185.

[9] LIU Y, LIN C, CHEN H, *et al.* A rapid Surface-Enhanced Raman scattering method for the determination of trace Hg^{2+} with tapered optical fiber probe[J]. Microchem. J., 2024(196).

[10] IBÁÑEZ-PALOMINO C, LOPEZ-SANCHEZ JF, SAHUQUILLO Ã. Inorganic mercury and methylmercury determination in polluted waters by HPLC coupled to cold vapour atomic fluorescence spectroscopy[J]. Int. J. Environ. Anal. Chem., 2012(92): 909 – 921.

[11] WU D, GORDON CK, SHIN JH, *et al.* Directed evolution of aptamer discovery technologies[J]. Acc. Chem. Res., 2022(55): 685 – 695.

[12] SUN L, LIU J, LI L, *et al.* Advances of biosensors for UO22 + detecting based on specific DNAzyme[J]. Inorg. Chem. Commun., 2022: 109234.

[13] ZHOU XL, ZHOU CH, GONG JY, *et al.* Novel thermo and ion-responsive copolymers based on metallo-base pair directed host-guest complexation for highly selective recognition of Hg^{2+} in aqueous solution[J]. J. Hazard. Mater., 2023(445): 130610.

[14] XU F, CHEN X, LV D, *et al.* Exonuclease III-assisted and target-induced conformational change of DNA hairpins for electrochemical detection of mercury (II) [J]. Microchem. J., 2024(196).

[15] QI Y, WANG Y, CHEN Y, *et al.* Rapid color-fading colorimetric sensing of Hg in environmental samples: regulation mechanism from DNA dimension[J]. Microchim. Acta, 2022(189): 76.

[16] ULLOA-GOMEZ AM, LUCAS A, KONERU A, *et al.* Simultaneous colorimetric and electrochemical detection of trace mercury (Hg^{2+}) using a portable and miniaturized aptasensor[J]. Biosens. Bioelectron., 2023 (221): 114419.

[17] LI D, LING S, CHENG X, *et al.* Development of a DNAzyme-based colorimetric biosensor assay for dual detection of Cd^{2+} and Hg^{2+} [J]. Anal. Bioanal. Chem., 2021(413): 7081 – 7091.

[18] XU X, CHEN J, HU R, *et al.* A dual-modality immunosensor for simple and reliable detection of nitrated alpha-synuclein in serum based on silver-coated MOF[J]. Microchim. Acta, 2023(190): 196.
[19] LI D, LV Y, XIA H, *et al.* Target-activated multivalent sensing platform for improving the sensitivity and selectivity of Hg^{2+} detection[J]. Anal. Chim. Acta, 2023(1256): 341123.
[20] HE W, QIAO B, LI F, *et al.* A novel electrochemical biosensor for ultrasensitive Hg^{2+} detection via a triple signal amplification strategy[J]. Chem. Commun., 2021(57): 619 – 622.
[21] HE YQ, CHEN Y, MENG XZ, *et al.* A versatile and smartphone-integrated detection platform based on Exo III-assisted recycling and DNAzyme amplification[J]. Sensor. Actuat. B: Chem., 2023(376): 132976.
[22] ZHANG D, WANG Y, JIN X, *et al.* A label-free and ultrasensitive electrochemical biosensor for oral cancer overexpressed 1 gene via exonuclease III-assisted target recycling and dual enzyme-assisted signal amplification strategies[J]. Analyst, 2022(147): 2412 – 2424.
[23] YANG DK, KUO CJ, CHEN LC. Synthetic multivalent DNAzymes for enhanced hydrogen peroxide catalysis and sensitive colorimetric glucose detection[J]. Anal. Chim. Acta, 2015(856): 96 – 102.
[24] TAN H, NAN Z. The high peroxidase-like activity of pyrite FS_2/SiO_2 hollow spheres for ascorbic acid detection[J]. Mater. Lett., 2022(320): 132280.
[25] CAO Y, LI W, PEI R. Exploring the catalytic mechanism of multivalent G-quadruplex/hemin DNAzymes by modulating the position and spatial orientation of connected G-quadruplexes[J]. Anal. Chim. Acta, 2022(1221): 340105.
[26] LI W, YANG X, HE L, *et al.* Self-assembled DNA nanocentipede as multivalent drug carrier for targeted delivery[J]. ACS Appl. Mater. Inter., 2016(8): 25733 – 25740.

Editor: Yingzhi GUANG Proofreader: Xinxiu ZHU

(Continued from page 14)

[10] ZHANG JJ, CHEN ZY, HAN Y, *et al.* Effects of different rootstocks on the growth and photosynthetic characteristics of 'Guiliyi' large-fruited Chinese chestnut seedlings[J]. China Agricultural Science and Technology Tribune, 2018, 20(03):10 – 19. (in Chinese).
[11] TIAN SL, SUN XL, SHEN GN, *et al.* Effects of urea and potassium dihydrogen phosphate co-application on photosynthetic characteristics, growth, and fruiting of chestnut trees[J]. Journal of Applied Ecology, 2015, 26(3): 747 – 754. (in Chinese).
[12] CHEN JP. Effects of manganese on the photosynthetic characteristics and mineral nutrition of 'Shimen Zao Shuo' chestnut[D]. Tai'an: Shandong Agricultural University, 2013. (in Chinese).
[13] FANG R, HUANG BL. Study on the photosynthetic characteristics of densely planted chestnut trees[J]. Journal of Zhejiang Forestry College, 1997(2): 43 – 46. (in Chinese).
[14] LI PF. Research and application of high – light efficiency breeding technology in crops[J]. Seed Science and Technology, 2006(6): 41 – 44. (in Chinese).
[15] YE ZP. A new model for relationship between irradiance and the rate of photosynthesis in Oryza sativa[J]. Photosynthetica, 2007(45): 637 – 640.
[16] LI L, ZHANG XX, ZHENG R, *et al.* Photosynthetic characteristics and fitting of light response curves in summer maize[J]. Acta Phytoecologica Sinica, 2016, 40(12): 1310 – 1318. (in Chinese).
[17] TIAN MY, DOU QQ, XIE YF, *et al.* Study on the photosynthetic characteristics of four thin – shell walnut varieties[J]. Journal of Nanjing Forestry University: Natural Sciences Edition, 2022, 46(5): 67 – 74. (in Chinese).
[18] LI D, HU DY, ZHAO HX, *et al.* Study on the photosynthetic characteristics and chlorophyll fluorescence characteristics of six ornamental bamboo species[J]. Shandong Agricultural Sciences, 2023, 55(7): 34 – 41. (in Chinese).
[19] ZONG SJ. Study on flowering, fruiting, and photosynthetic characteristics of six superior Chinese chestnut varieties[D]. Central South University of Forestry and Technology, 2022. (in Chinese).
[20] ZHANG H. Study on the photosynthetic characteristics of two hawthorn varieties[J]. Journal of Fruit Resources, 2023, 4(3): 47 – 51. (in Chinese).
[21] ZHANG Y, HAN LQ, ZHAO Y, *et al.* Comparison of leaf structure and photosynthetic characteristics of two main walnut varieties in Xinjiang[J]. Economic Forest Research, 2022, 40(2): 153 – 163, 182. (in Chinese).
[22] YANG W, YU ZY, LI XG. Study on the photosynthetic characteristics of three strawberry varieties[J]. Northern Horticulture, 2015(10): 50 – 53. (in Chinese).
[23] LIU QZ, DONG HM, LIU P, *et al.* Study on the photosynthetic characteristics of chestnut trees[J]. Journal of Fruit Science, 2005, 22(4): 335 – 338. (in Chinese).
[24] ZHANG Y, SHAO JZ, LIU XJ, *et al.* Research progress on photosynthesis in Chinese chestnut[J]. Journal of Northwest Forestry University, 2007, 22(5): 53 – 56. (in Chinese).
[25] XIAO NJ, SHI YC, WEI X, *et al.* Fitting of light response models and study on photosynthetic characteristics of three vine medicinal and edible plants[J]. Tropical Agricultural Sciences, 2023, 43(9): 13 – 21.
[26] LU B, ZHENG YQ, WEI B, *et al.* Comparative study on diurnal variations of photosynthesis in three Hakeleirei holly varieties[J]. Forestry and Environmental Science, 2023, 39(2): 59 – 66. (in Chinese).
[27] WU AJ, XU WZ, GUO YL, *et al.* Characteristics of photosynthesis – light response curves of Daurian buckthorn under different water and fertilizer conditions[J]. Acta Prataculturae Sinica, 2015, 23(4): 785 – 792. (in Chinese).
[28] WANG M, NING DL, LI XZ, *et al.* Research overview on thin – shell walnuts[J]. China Forestry Science and Technology, 2010(2): 84 – 86. (in Chinese).
[29] WANG J, MO HR, *et al.* Analysis of light response curve characteristics of 10 Plantago species[J]. Anhui Agricultural Sciences, 2015, 43(33): 23 – 26, 39. (in Chinese).
[30] ZHANG YH. Light response curve characteristics of three introduced ornamental tree species[J]. Forestry Survey and Design, 2019, 39(1): 1 – 4. (in Chinese).
[31] TANG XL, JIANG J, JIN HP, *et al.* Effects of shading on chlorophyll content and photosynthetic characteristics of *Machilus minuta*[J]. Chinese Journal of Applied Ecology, 2019, 30(9): 2941 – 2948. (in Chinese).
[32] HE HY, PENG FR, ZHANG R, *et al.* Comparative study on photosynthetic characteristics of grafted seedlings of different varieties of *Juglans nigra*[J]. Journal of Nanjing Forestry University: Natural Sciences Edition, 2015, 39(4): 19 – 25. (in Chinese).

Editor: Yingzhi GUANG Proofreader: Xinxiu ZHU